



Self-assembly of various Au nanocrystals on functionalized water-stable PVA/PEI nanofibers: A highly efficient surface-enhanced Raman scattering substrates with high density of “hot” spots

Han Zhu^a, MingLiang Du^{a,b,*}, Ming Zhang^{a,b}, Pan Wang^a, ShiYong Bao^a, Meiling Zou^a, YaQin Fu^{a,b}, JuMing Yao^{a,b}

^a Department of Materials Engineering, College of Materials and Textile, Zhejiang Sci-Tech University, Hangzhou 310018, PR China

^b Key Laboratory of Advanced Textile Materials and Manufacturing Technology, Zhejiang Sci-Tech University, Ministry of Education, Hangzhou 310018, PR China

ARTICLE INFO

Article history:

Received 17 August 2013
Received in revised form
8 October 2013
Accepted 22 October 2013
Available online 31 October 2013

Keywords:

Self-assembly
Au nanocrystals
Nanofibers
SERS

ABSTRACT

We have demonstrated a facile approach for the fabrication of flexible and reliable sulfhydryl functionalized PVA/PEI nanofibers with excellent water stability for the self-assembly of Au nanocrystals, such as Au nanoparticles (AuNPs), Au nanoflowers (AuNFs) and Au nanorods (AuNRs), used as the highly efficient surface-enhanced Raman scattering (SERS) substrates for the detection of rhodamine B (RhB). Various methods were employed to cross-link the PVA nanofibers with better morphology and porous structures after immersing in water for desired times. Various SERS-active Au nanocrystals, such as AuNPs, AuNFs, and AuNRs have been successfully synthesized. After the grafting of MPTES on the cross-linked PVA/PEI nanofibers, the Au nanocrystals can easily be self-assembled on the surfaces of the nanofibers because of the strong interactions of the Au–S chemical bondings. The Au nanocrystals self-assembled throughout the PVA/PEI nanofibers used as SERS substrates all exhibit enhanced SERS signals of RhB compared with their individual nanocrystals. It is mainly due to the close interparticle distance, mutual orientation and high density of “hot” spots, that can strongly affect the overall optical response and the SERS enhancement. By changing the amounts of the self-assembled AuNFs on the nanofibers, we can control the density of the “hot” spots. With the increased amounts of the AuNFs throughout the nanofibers, the SERS substrates show enhanced Raman signals of the RhB, indicating that the increased density of “hot” spots can directly lead to the SERS enhancement. The AuNFs/(PVA/PEI) SERS substrates show good sensitivity, reliability and low detection limit (10^{-9} M). The presented approach can be broadly applicable to the assembly of different types of plasmonic nanostructures and these novel materials with strong SERS enhancement can be applied in bioanalysis and biosensors.

© 2013 Elsevier B.V. All rights reserved.

1. Introduction

Surface-enhanced Raman scattering (SERS) is a powerful technique for the trace level detection of various biological and chemical species and would promise to make a huge impact in life sciences, environmental monitoring, and homeland security (Wang et al., 2013, 2012b; Gong et al., 2012; Fan et al., 2013; Kim et al., 2011; Lee et al., 2011). This is not only due to its high sensitivity but also because SERS provides vibrational (fingerprint) information of target molecules. Recently, due to the versatility in surface modification, bio-inertness, and remarkable optical

properties known as localized surface plasmon resonance (LSPR), Au nanostructures have created a great promise for their use in a variety of electronic, optical, and biomedical applications, catalysts and SERS substrates (Vigderman et al., 2012; Engel et al., 2012; Saha et al., 2012b; Aragay et al., 2012; Xiao et al., 2010; Personick et al., 2011; Perez-Juste et al., 2005; Xie et al., 2011). One of the most active research fields in SERS substrates is related to the quest for new substrates with improved enhancement efficiency and reproducibility. These efforts include several approaches, such as the development of new nanomaterials by top-down methods and the self-assembly of nanoparticles (NPs) in planar platforms (Fan et al., 2013; Anker et al., 2008; Fan and Brolo, 2009).

Assembly of individual NPs into a nanostructured hierarchy is emerging as a crucial step toward their integration within devices, which is a frontier area of research in modern chemistry and materials science (Zhang et al., 2012a; Kotov 2011; Sanchez-Iglesias et al., 2010).

* Corresponding author at: Department of Materials Engineering, College of Materials and Textile, Zhejiang Sci-Tech University, Hangzhou 310018, PR China. Tel.: +86 571 86843763.

E-mail addresses: du@zstu.edu.cn, psduml@gmail.com (M. Du).

For example, even though the individual NPs are shown to exhibit a modest SERS effect, and while the metal nanostructures assembled in an organized manner with extremely small (typically less than 5 nm) interparticles spacing, it would result in significantly large SERS enhancement due to the strong capacitive coupling (Lee et al., 2011; Liu et al., 2013; Xie and Schlucker, 2013; Rycenga et al., 2011). This effect is largely influenced by the polarization of incident light relative to different interparticle vectors, with the polarization parallel to interparticle axis resulting in the largest SERS enhancement (Lee et al., 2011; Moskovits, 2005). When the analyte molecules are trapped in the interstitial sites, the “hot spots” formed between the assembled nanostructures and experienced enormous localized electromagnetic field, which effectively results in large SERS enhancement. It is well-known that the “hot” spots make a major contribution to SERS, and the enhancement due to the assembled NPs is about six orders of magnitude higher than for isolated NPs (Liu et al., 2013; Qian et al., 2012; Saha et al., 2012a). Although self-assembly has been widely studied, the fabrication of controllable and reproducible “hot” spots is still a major challenge.

Up to date, support-assisted self-assembly of nanostructures has drawn more attention because of their high densities and reproducible “hot” spot structures. Silica, carbon nanotubes, and inorganic nanowires are commonly used as support materials for depositing metal NPs (Peng et al., 2011; Schmit et al., 2012; Yoon et al., 2009; Yuan et al., 2009). For example, Schmit et al. described a new class of materials for SERS consisting of gold NPs coated onto hollow, buoyant silica microspheres and these SERS-active nanomaterials exhibit a low detection limit of ~ 170 ppt for cyanide (Schmit et al., 2012). As one of the 1-D substrates, electrospun polymer nanofibers gradually attracted the attention of many researchers because of the associated advantages of the synthesizing technique and the obtained product. There are several remarkable characteristics such as extremely large surface area to volume ratio, flexibility in surface functionalities, high porosity and superior mechanical performance, compared with the carbon nanotubes, metal and metal oxide nanowires, making the polymer nanofibers optimal candidates for self-assembly of nanocrystals (Destaye et al., 2013; Wang et al., 2012a; Peng et al., 2012; Liu et al., 2011; Zhu et al., 2013b, 2013c). Recently, Yu et al. have demonstrated a facile way for the fabrication of arranged Ag nanoparticles (AgNPs) and Au nanorods (AuNRs) embedded in poly(vinyl alcohol) (PVA) nanofibrous mats by electrospinning, both exhibiting high SERS enhancement (Zhang et al., 2012a; He et al., 2009). Meanwhile, Schlucker et al. have reported that the SERS enhancement also has a strong analyte distance-dependence feature – only molecules on or very close to the metal surface experience the enormous field enhancement (Wang et al., 2013; Schlucker, 2009). However, the metal nanocrystals embedded in the PVA nanofibers may restrict the close distance between the analyte molecules and the nanocrystals, resulting in weak SERS enhancement. In addition, in Yu's studies, the substrates PVA nanofibers were water-soluble and cannot be applied in water environment, which may impose restrictions on their practical applications.

In our previous studies, our groups have shown that uniform and well-dispersed Au and AgNPs can be immobilized on the amino-functionalized halloysite nanotubes via in situ reduction and these novel materials exhibit high catalytic activity and strong SERS enhancement (Zhu et al., 2012b; 2012c). In addition, we also fabricated the sulfhydryl functionalized water-stable PVA nanofibers to served as a nanoreactor for the in situ growth of AgNPs, and the fabricated AgNPs/PVA nanofibers have been demonstrated to be a highly active biosensor for the detection of glutathione and glucose (Zhu et al., 2013b, 2013c). The previous studies lead us to develop a combined self-assembly and templating technique to construct various nanostructured arrays of metal nanocrystals.

The combination of hybrid aggregated nanostructures displays distinct optical and electrical properties compared with their individual components. Such hybrid structures show promise for applications in SERS substrates, electronics, optics, and photovoltaic cells (Huang et al., 2010; Zhang et al., 2010; Song et al., 2010).

Here, we reported flexible and reliable sulfhydryl functionalized PVA/PEI nanofibers with excellent water stability for the self-assembly of Au nanocrystals, such as AuNPs, Au nanoflowers (AuNFs), AuNRs, using the highly efficient SERS substrates for the detection of rhodamine B (RhB). For the aim of practical applications, various methods were employed to cross-link the PVA nanofibers with better morphology and porous structures after immersing in water for the desired time. Fourier transform infrared spectra (FTIR) and X-ray photoelectron spectrometer verified the linkage bondings of the cross-linked nanofibers. Various SERS-active Au nanocrystals, such as AuNPs, AuNFs, and AuNRs have been successfully synthesized. After the grafting of 3-mercaptopropyl-trimethoxysilane (MPTES) on the cross-linked PVA/PEI nanofibers, the Au nanocrystals can easily be self-assembled on the surfaces of the nanofibers because of the strong interactions of the Au–S chemical bondings. The amount of the Au nanocrystals on the nanofibers can be adjusted by changing the concentration of the nanocrystals solution. Therefore, with the fine formation of nanocrystal junctions, aggregates can produce intense Raman signatures of reporters with high reproducibility. The AuNFs with multibranch nanostructures exhibit higher SERS enhancement for the detection of RhB, due to more surface roughness and extremely small radii of curvature, resulting in strong electric field enhancement and subsequently large SERS enhancement factors per surface molecule, which is referred to as a “sharp tip effect”. The Au nanocrystals self-assembled throughout the PVA/PEI nanofibers as SERS substrates all exhibit enhanced SERS signals of RhB compared with their individual nanocrystals. It is mainly the close interparticle distance, mutual orientation and high density of “hot” spots, that can strongly affect the overall optical response and the SERS enhancement. By changing the amounts of the self-assembled AuNFs on the nanofibers, we can control the density of the “hot” spots and with the increased amounts of the AuNFs throughout the nanofibers, the SERS substrates show enhanced Raman signals of the RhB, indicating that the increased density of “hot” spots can directly lead to the SERS enhancement. The AuNFs/(PVA/PEI) SERS substrates show good sensitivity, reliability and low detection limit (10^{-9} M). The presented approach can be broadly applicable to different types of plasmonic nanostructures and these novel materials with strong SERS enhancement can be applied in bioanalysis and biosensors.

2. Material and methods

2.1. Materials

The materials information used in this paper is shown in [Supporting information](#).

2.2. Fabrication of the water-stable PVA nanofibrous mats

In the fabrication of PVA/GA nanofibers, the GA solution (30 wt%) was mixed with the PVA aqueous solution (10 wt%) under vigorous stirring to achieve a homogeneous solution, in which the mass ratio of PVA and GA was 4:1. The as-prepared PVA/GA electrospun precursor solution was collected in a 10 mL syringe equipped with a 24 gage stainless steel needle tip. The syringe was fixed on an electric syringe pump set to maintain constant feed rate of 0.01 mL min^{-1} for PVA/GA nanofibers. The voltage was

12 kV and the distance between the needle tip and the collector were 12 cm.

In the fabrication of the cross-linked PVA nanofibers via GA vapor, the PVA precursor solution (10 wt%) was firstly electrospun into the PVA nanofibers, and then treated via the GA vapor in a vacuum oven at 60 °C for 24 h.

For the preparation of cross-linked PVA/PEI electrospun precursor solution, PEI (50 wt%) and PVA (12 wt%) solutions were mixed together under magnetic stirring overnight with a PEI/PVA mass ratio of 1:3 to achieve a homogeneous solution. The electrospun procedure of PVA/PEI precursor was similar to PVA/GA nanofibers. The constant of the feed rate, voltage and distance are 0.005 mL min⁻¹, 20 kV and 20 cm respectively. The freshly prepared PEI/PVA nanofibers were then cross-linked by GA vapor to render the nanofibers with water stability. The diameters and distribution of all the prepared nanofibers were measured by Image-Pro Plus6.2 software (200 nanofibers were randomly selected for the measurement).

2.3. Facile synthesis of the various Au nanocrystals

A green and facile approach was used to synthesize the AuNPs. In brief, 10 mL Au (III) solution (5.0 mmol L⁻¹) and 90 mL water were first injected into a 3-neck flask (fitted with a reflux condenser and a Teflon-coated stir bar) under vigorous stirring by magnetic force at 65 °C. Then, 0.025 g EGCG dissolved in 5 mL water were injected into the above Au (III) solution and the mixture was kept refluxing for 3 h to form homogeneous AuNPs in aqueous solution. The obtained AuNPs aqueous solution was transferred into a beaker after cooling to room temperature and stored at 4 °C in a refrigerator before use.

In a typical experiment to synthesize AuNFs, 1 mL of 100 mM HEPPS (pH 7.4) was mixed with 9 mL of water, followed by the addition of 500 µL of 20 mM HAuCl₄ solution. The color of solution changed from light yellow to pink and finally to turbid blue under ambient environment within 30 min without disturbing.

The AuNRs were prepared according to the seed growth method with a slight adjustment (Park et al., 2013). Briefly, the seed solution was made by adding a freshly prepared, ice-cold NaBH₄ solution (0.6 mL, 0.01 M) into a solution composed of HAuCl₄ (0.025 mL, 0.1 M) and CTAB (10 mL, 0.1 M). The growth solution was prepared separately by mixing HAuCl₄ (500 µL, 0.1 M), AgNO₃ (100 µL, 0.1 M), and CTAB (100 mL, 0.1 M), at room temperature. Next, ascorbic acid (600 µL, 0.1 M) was added to the growth solution as a mild reducing agent. Finally, 100 µL of the seed solution aged for 5 min was added into the growth solution.

2.4. Self-assembly of the Au nanocrystals on the MPTES functionalized PVA/PEI nanofibers

For the functionalization of the PVA/PEI nanofibers by MPTES, the water-stable nanofibrous mats were immersed into the MPTES ethanol solution (10 vol%) by vigorous shaking in an incubator shaker at 40 °C for 12 h and then rinsed with DIW and ethanol three times. The freshly washed nanofibrous mats were immersed into the desired volume of Au nanocrystals aqueous solution (AuNPs, 10 mL; AuNFs 12 mL, AuNRs, 8 mL) followed by vigorous shaking in an incubator shaker at 40 °C for 3 h until the Au nanocrystals aqueous solution changed to colorless. The fabricated nanofibrous mats were rinsed with DIW three times, followed by drying at room temperature. The diameters and distributions of the Au nanocrystals were measured by Image-Pro Plus6.2 software (200 particles were randomly selected for the measurement).

2.5. SERS experiments

RhB was chosen as a model analyte to investigate the performance of the Au nanocrystals assembled on the PVA/PEI nanofibers as a substrate for SERS detection. The AuNPs, AuNFs, and AuNRs solution was mixed with the RhB solution (1 mL, 10⁻⁵ M) for 12 h to make the adsorption equilibrium of RhB on the Au nanocrystals. Similarly, the SERS measurements were performed by dropping 1 mL of RhB solution (10⁻⁵ M) onto the PVA/PEI nanofibers with Au nanocrystals assembled substrates. Then, the nanofibers substrates mat was washed thoroughly with water to remove unbound RhB molecules and finally dried at room temperature to evaporate all of the water.

2.6. Instrumentation

Transmission electron microscopy (TEM) images were obtained with a JSM-2100 transmission electron microscopy (JEOL, Japan) at an acceleration voltage of 200 kV. The EDS spectrum of the AuNFs/(PVA/PEI) nanofibers was also recorded by the TEM. The morphologies of all the electrospun nanofibers were observed by a JSM-6700F field-emission scanning electron microscope (FE-SEM, JEOL, Japan) at an acceleration voltage of 1 kV. X-ray Diffraction (XRD) patterns of the PVA/PEI nanofibers with and without Au nanocrystals were characterized with a SIEMENS Diffraktometer D5000 X-ray diffractometer using Cu Kα radiation source at 35 kV, with a scan rate of 0.02° 2θ s⁻¹ in the 2θ range of 10–80°. Fourier transform infrared (FTIR) spectra were recorded on a Nicolet 5700 FTIR spectrometer in transmittance mode at a resolution of 4 cm⁻¹ and 32 scans in the range from 4000 nm to 400 nm. The as-prepared AuNPs, AuNFs and AuNRs aqueous solution were examined by a Lambda 900 UV–vis spectrophotometer (Perkin Elmer, USA). All the spectra were collected over a wavelength range of 200–800 nm. Thermogravimetric analysis (TGA; Pyris 1) was carried out from 298 to 1073 K at a heating rate of 5 K/min in N₂ atmosphere. X-ray photoelectron spectra of cross-linked PVA/PEI nanofibers, MPTES functionalized PVA/PEI nanofibers and AuNFs/(PVA/PEI) nanofibers were recorded using an X-ray Photoelectron Spectrometer (Kratos Axis Ultra DLD) with an aluminum (mono) Kα source (1486.6 eV). The aluminum Kα source was operated at 15 kV and 10 mA. Raman spectra of all the samples were recorded by a Renishaw inVia Raman microscope using a 785 nm laser excitation source. The excitation light intensity in front of the objective was 10 mW with a spectral collection time of 1 s for SERS experiments. The integration time for our measurements was set to 10 s.

3. Results and discussion

The polymer nanofibers substrate with good morphology, water stability and porous structures for the self-assembly of Au nanocrystals is a prerequisite factor for the fabrication of reliable and reproducible SERS substrates. To retain their water stability, three different methods were utilized to cross-link the PVA nanofibers. The PVA/GA nanofibers were firstly prepared from the PVA/GA solution and, as shown in Fig. 1a, uniform and smooth nanofibers without any adhesion can be obtained. The average diameter of the PVA/GA nanofibers is 260 ± 42 nm (Fig. S1). However, when the obtained PVA/GA nanofibrous mats were immersed in water, it was found to instantaneously dissolve in water and swell considerably. As shown in Fig. 1d, the nanofibers start to fuse with each other and destroy porous openings of the nanofibrous mats.

It is should be noted that maintaining the nanofiber morphology and porous structure of nanofibers mats is important for the

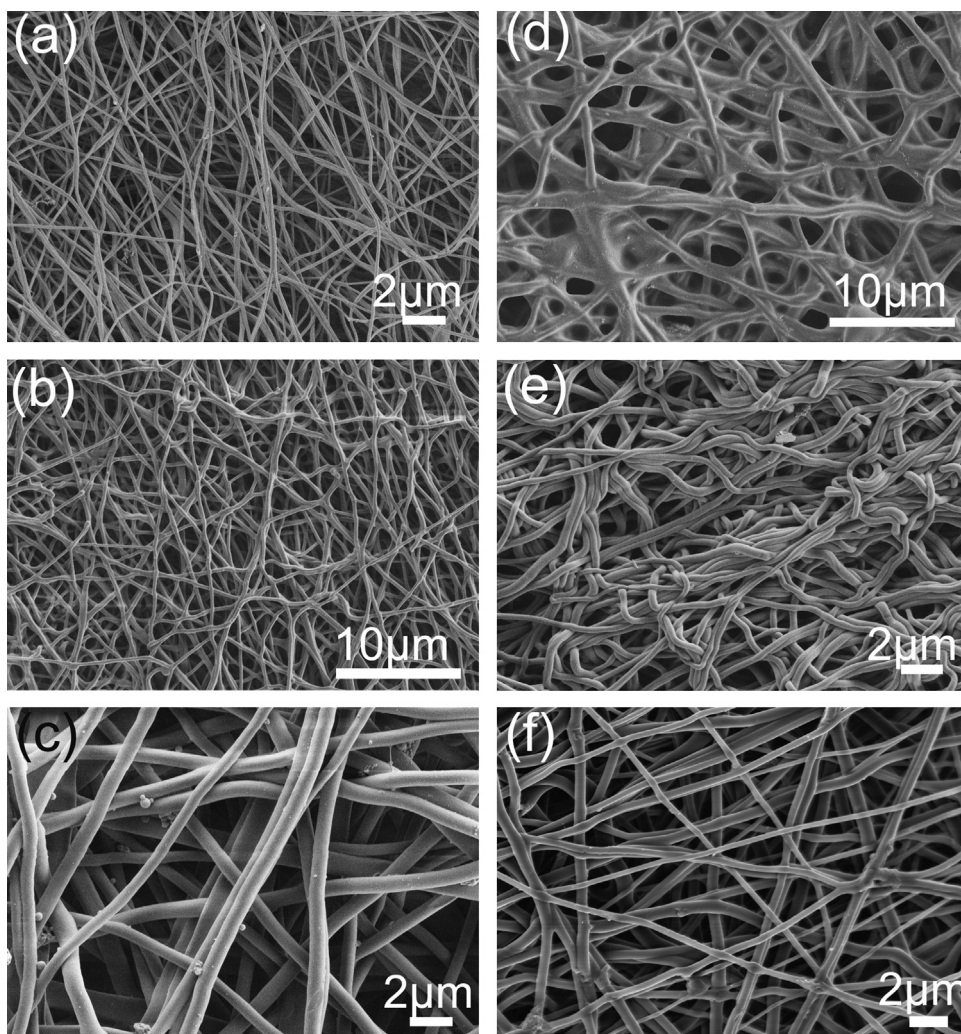


Fig. 1. FE-SEM images of the (a) fresh PVA/GA nanofibers, (b) cross-linked PVA nanofibers via GA vapor, and the (c) cross-linked PVA/PEI nanofibers via GA vapor. The FE-SEM images of the corresponding nanofibers immersed in water for (d) 30 min, (e) 24 h, and (f) 72 h.

practical applications where a high surface-area-to-volume ratio is considered advantageous (Destaye et al., 2013). After the treatment by GA vapor, as shown in Fig. 1b, the originally straight nanofibers become merged and entangled among each other and form interfiber bonding/fused mostly at the intersection points. It is because the GA vapor contains water vapor and it could soften and swell the surfaces of the nanofibers, leading to the direct contact with nearby nanofibers at intersection points and then the formation of interfiber bondings. When the GA vapor cross-linked PVA nanofibrous mats were immersed in water for 24 h, as shown in Fig. 1e, the phenomena of the merged and entangled nanofibers become serious and compared with Fig. 1b, the porous structures were destroyed. Through the GA vapor treatment, the water stability of the nanofibers can be improved; however, the porous structures cannot withstand the water. Fig. 1c shows the cross-linked PVA/PEI nanofibers via GA vapor, smooth and uniform PVA/PEI nanofibers with random orientation were obtained with an average diameter of 510 ± 50 nm (Fig. S2). There are no significant merged and entangled nanofibers instead of interfiber bonding/fused nanofibers at the intersection points with excellent porous nanofibers. After immersing in water for 72 h, as shown in Fig. 1f, the water-insoluble PVA/PEI nanofibrous mats were still well preserved and kept excellent porous fiber structure, suggesting the successful cross-linking reaction to form aldime linkages between the free amino groups of PEI and the GA (Destaye et al.,

2013; Zhu et al., 2013c). The cross-linkages of the PVA/GA and PVA/PEI nanofibers are characterized by FTIR spectra, and the information and discussion are shown in Supporting information (Fig. S3).

Three different morphologies of the Au nanocrystals with SERS activity have been successfully synthesized, which are AuNPs, AuNRs, and AuNFs. For the synthesis of AuNPs, unlike the most widely used sodium citrate methods, our groups have introduced the natural tea polyphenols (TP) to act both as reducer and stabilizer to synthesize Au and AgNPs (Zhu et al., 2012c; Zou et al., 2013). In the present investigation, we use the main ingredient of TP, epigallocatechin gallate (EGCG), both as the reducer and stabilizer to synthesize AuNPs. As shown in Fig. 2a, relatively uniform AuNPs with an average diameter about 20.2 ± 2.6 nm (Fig. S4) are well-dispersed in water without any aggregations, indicating the reliable stabilization of the EGCG.

Fig. 2d exhibits that the AuNPs are mainly composed of (111) planes with a d-spacing of 0.23 nm, which could be indexed by the face-centered cubic (fcc) structure of Au crystals (Zhu et al., 2012a, 2013a). The selected-area electron diffraction (SAED) of the AuNPs reveals diffraction rings indexed to the (111), (200), (222), and (311) planes of fcc gold, respectively, indicating the polycrystallinity of AuNPs (Du and He, 2010). The AuNRs were prepared using a seed-mediated growth method in aqueous solutions and are stabilized with CTAB. As shown in Fig. 2b, the shapes and sizes of

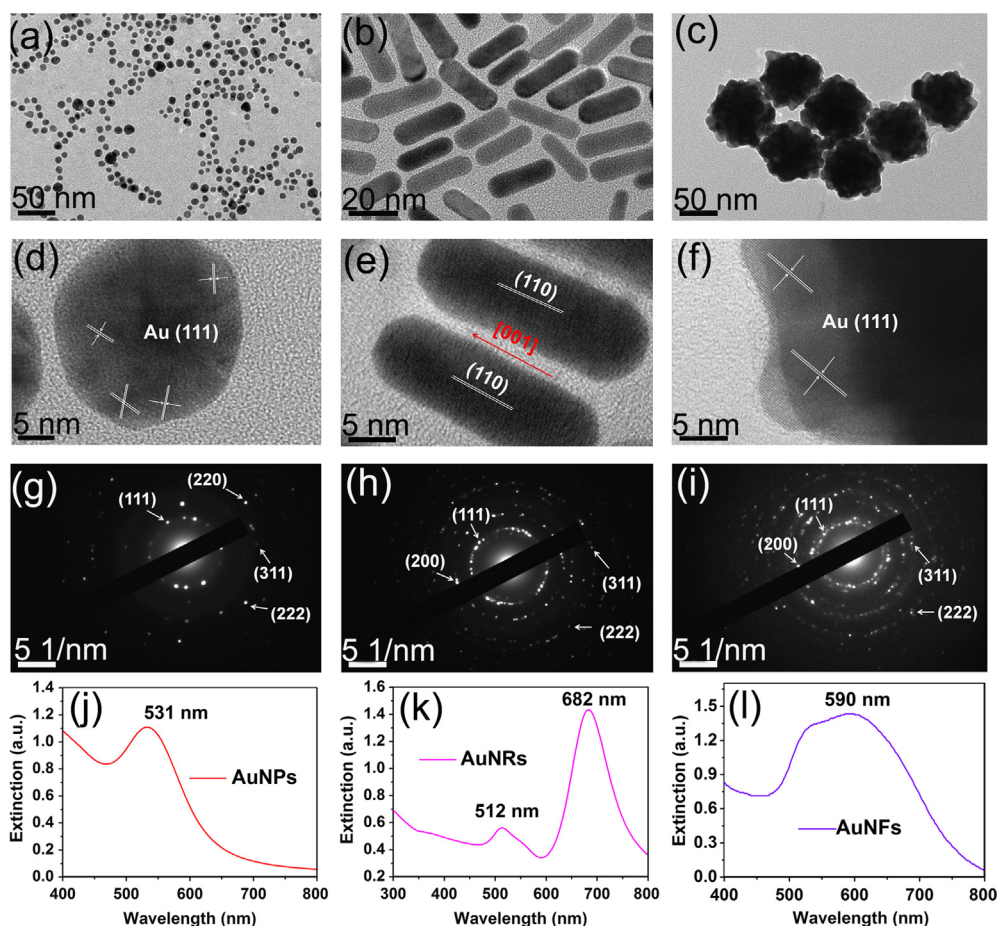


Fig. 2. TEM and HRTEM images of the (a) and (d) AuNPs, (b) and (e) AuNRs, and (c) and (f) AuNFs. The corresponding SAED patterns of the (g) AuNPs, (h) AuNRs, and (i) AuNFs. The UV-vis spectra of the (j) AuNPs, (k) AuNRs and (l) AuNFs solution.

the nanorods samples are relatively uniform with an average radius of $r_{rod}=7$ nm and an average length of $l_{rod}=35$ nm.

Fig. 2e shows that the AuNRs are single-crystalline, growing along the [001] direction. The SAED of the AuNRs indicates diffraction rings indexed to the (111), (220), (222), and (311) planes of fcc gold (Singh et al., 2013). For the synthesis of AuNFs, a common Good's buffer in chemistry and biochemistry, HEPES, could be used as a weak reducing agent in AuNFs synthesis. Fig. 2c shows the typical TEM image of the AuNFs synthesized in 10 mM HEPES solution. The as-synthesized AuNFs are quasi-spherical, consisting of a solid Au core with many short, irregular, and obtuse Au nanocrystals. The diameter of the quasi-spherical AuNFs varies from 50 to 80 nm, and the Au nanocrystals around the Au cores have a variety of shapes and sizes. The HRTEM image (Fig. 2f) shows that the short, irregular, and obtuse Au nanocrystals which protruded from the core of the nanoflowers are single-crystalline and the distinct lattice fringes with a d-spacing of 0.23 nm correspond to the (111) planes of fcc gold. The SAED pattern shows that the AuNFs are crystalline and randomly oriented (He et al., 2012; Zhang et al., 2011; Xie et al., 2008).

Fig. 2j shows a sharp absorption peak located at the 531 nm, which is believed to be a consequence of photoexcitation of the free conduction electrons on the surface of AuNPs (Zhu et al., 2012c; Zou et al., 2013). The characteristic surface plasmonic resonance (SPR) band of AuNPs is relatively narrow, suggesting a good dispersion and narrow size distribution of AuNPs. As for AuNRs, Fig. 2k shows a longitudinal SPR peak at 682 nm and a transverse one at 512 nm (Ye et al., 2012; Jiang et al., 2012; Qiao et al., 2011). Similarly, the extinction spectrum of AuNFs indicates

a broad SPR peak located around 590 nm, which is shown in Fig. 2l. All the extinction spectra can confirm the successful synthesis of the Au nanocrystals.

The cross-linked PVA/PEI nanofibers were firstly functionalized by MPTES, and then used as the substrates for the self-assembly of the Au nanocrystals, which are AuNPs, AuNRs, and AuNFs. As shown in Fig. 3a and b, uniform AuNPs are evenly dispersed throughout the PVA/PEI nanofibers. The AuNPs are attached to the surfaces of the nanofibers and there are no obvious aggregated AuNPs, indicating the strong chemical bonding between the AuNPs and the -SH groups. For the self-assembly of the AuNFs, large amount of the AuNFs were densely immobilized on the surfaces of the PVA/PEI nanofibers, which are shown in Fig. 3c and d. As shown in Fig. 3e and f, a portion of the independent AuNRs can be observed immobilized on the PVA/PEI nanofibers. However, relatively serious aggregated AuNRs are emerged on the PVA/PEI nanofibers. It is because in the synthesis of AuNPs and AuNFs, EGCG and HEPES are both used as the reducer and the capping agents, and they are weak capping agents, while the CTAB is a strong capping agents.

There is a competition between these capping agents and thiol groups on the nanofibers surface. When different processes of bindings compete, the binding leading to the maximum decrease in the surface energy prevails. Therefore, the good dispersion of Au nanocrystals on the nanofibers surface strongly depends on the ability of the thiol groups modified surface to displace the stabilizer at the surface of Au nanocrystals. As for the weak capping agents, the AuNPs and AuNFs showed a homogeneous distribution over the MPTES functionalized nanofibers due to the

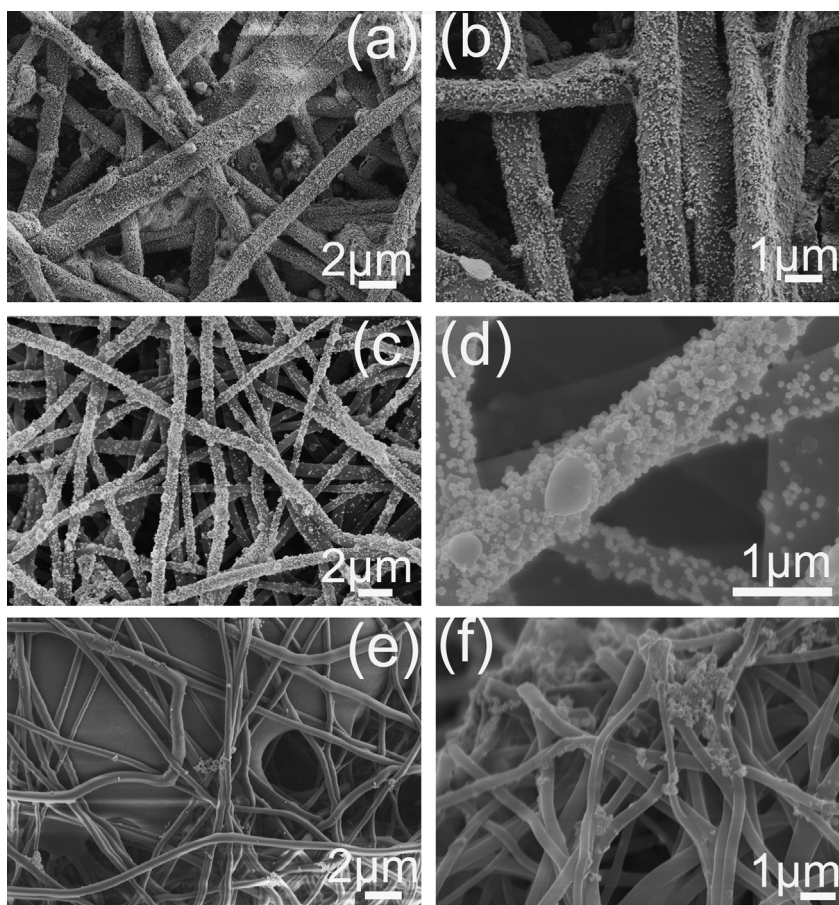


Fig. 3. FE-SEM images of the self-assembly of the (a) and (b) AuNPs, (c) and (d) AuNRs, and (e) and (f) AuNFs on the MPTES functionalized PVA/PEI nanofibers.

strong Au–S bondings. The CTAB-stabilized AuNRs showed a poor adsorption and aggregated AuNRs on MPTES functionalized PVA/PEI nanofibers. This is probably because of the high stability of the CTAB bilayers around the particles and the combined effect of charge repulsion between thiol groups and quaternary ammonium (Tamoto et al., 2012).

The FTIR spectra, XRD patterns and TG curves of the fabricated Au nanocrystals self-assembled on the MPTES functionalized PVA/PEI nanofibers are discussed in Supporting information (Figs. S5 and S6).

XPS spectra were used to study the chemical bondings and illustrate the chemical changes between the MPTES grafting and the self-assembly process. Fig. 4a and b show the C 1s XPS spectra of the cross-linked PVA/PEI and MPTES functionalized PVA/PEI nanofibers. As shown in Fig. 4a, four distinct XPS peaks are observed, indicating four different binding energies (BEs) of C 1s. The primary C1s peak, located at 284.7 eV, was ascribed to the C–C backbone of the PVA/PEI (Chen et al., 2011; He et al., 2011; Khatri et al., 2008). The 286.6 eV peak was mainly attributed to the carbon atoms of the carbonyl group (C=O) as well as the carbon atoms adjacent to the amide bond (C–NH₂) (Tamoto et al., 2012). The fitted peak at 287.5 eV was also attributed to carbon atoms adjacent to the amide bond (C–NHR) in PEI. In addition, the C peak with BE at 289.7 eV is attributed to the carbon atoms of aldimine groups as well as the ester group (Chen et al., 2011; He et al., 2011). The XPS results can demonstrate the formation of the aldimine groups, indicating the successful cross-linkages of the PVA/PEI nanofibers. Comparing Fig. 4b with a, similar C 1s peaks can be observed and the peaks are located at 284.7, 285.9, 287.8, and 289.0 eV, respectively. The C 1s XPS spectrum of the MPTES functionalized PVA/PEI nanofibers shows a new emerged peak

with BE at 290.7 eV which is attributed to the carbon atoms of C–O–Si groups in MPTES, indicating the successful grafting of MPTES on PVA/PEI nanofibers (He et al., 2011; Khatri et al., 2008). As shown in Fig. 4c and d, the O 1s spectra of the PVA/PEI nanofibers with and without MPTES both exhibit a strong peak with BE at 532.4 eV, belonging to the C–OH groups in PVA.

Fig. 4d exhibits two chemical states of the O 1s, and the weaker O 1s peak located at 533.8 eV is ascribed to the Si–O groups, confirming the grafting of MPTES on nanofibers. As shown in Fig. 4e, the appearance of characteristic Si 2p peaks at 102.1 eV, Si 2p_{1/2} at 98.0 eV, and Si 2p_{3/2} at 96.9 eV, which are ascribed to the Si–O, Si–C and Si–Si bondings (Selegard et al., 2010; Wang et al., 2004). The presence of Si–O bondings can successfully confirm the grafting between –OH groups in PVA and Si–C groups in MPTES. The above XPS results can strongly support the successfully cross-linkages of the PVA/PEI nanofibers and the grafting reaction between the MPTES and the –OH groups. The Au–S bondings generated between the –SH groups in MPTES and the Au nanocrystals and the formation of the Au–S bondings are the key factor for the self-assembly process. The S 2p XPS spectra of the MPTES functionalized PVA/PEI nanofibers before and after the self-assembly of Au nanocrystals were used to study the Au–S bondings.

As shown in Fig. 4f, the XPS S 2p core level spectrum of MPTES functionalized PVA/PEI nanofibers exhibits a pair of peaks, which are ascribed to the spin–orbit-splitting doublet with the S 2p_{3/2} and S 2p_{1/2} BE positions at 163.8 and 164.8 eV, respectively (Selegard et al., 2010; Wang et al., 2004). This is consistent with the binding energy of unbound thiol (–SH) groups, which is in accord with the previously reported literatures (Zhu et al., 2013b; Selegard et al., 2010). As for the analysis of the AuNFs/(PVA/PEI)

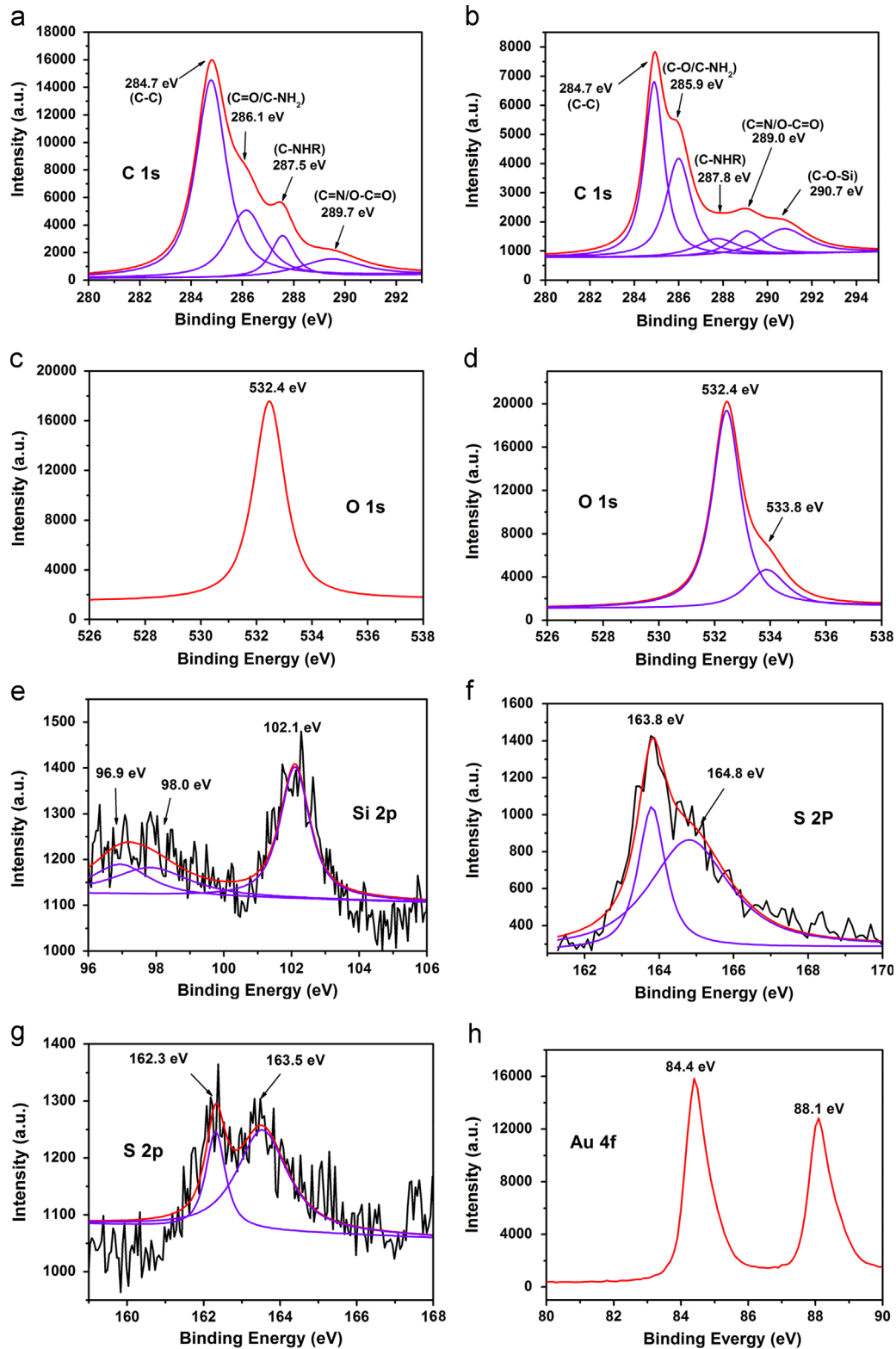


Fig. 4. C 1s XPS spectra of the (a) cross-linked PVA/PEI and (b) MPTES functionalized PVA/PEI nanofibers. O 1s XPS spectra of the (c) cross-linked PVA/PEI and (d) MPTES functionalized PVA/PEI nanofibers. Si 2p XPS spectra of the (e) MPTES functionalized PVA/PEI nanofibers. S 2p XPS spectra of the (f) MPTES functionalized PVA/PEI and (g) AuNFs/(PVA/PEI) nanofibers. (h) Au 4f XPS spectra of the AuNFs/(PVA/PEI) nanofibers.

nanofibers sample, the observed doublet peaks of S 2p_{3/2} and S 2p_{1/2} with the BEs at 162.3 eV and 163.5 eV, respectively, are corresponding to thiolate species, confirming the formation of the Au–S bondings (Zhu et al., 2013b; Selegard et al., 2010). In addition, the Au 4f XPS spectrum of the AuNFs/(PVA/PEI)

nanofibers shown in Fig. 4h exhibits two sharp and distinct peaks located at 88.1 eV and 84.4 eV and they are in agreement with the binding energies of Au 4f_{7/2} and Au 4f_{5/2}, respectively (Zhu et al., 2012c, 2013a). Compared with the BEs of Au⁰ (87.7 eV and 84.0 eV), the shifts in the BE indicate the strong Au–S bondings

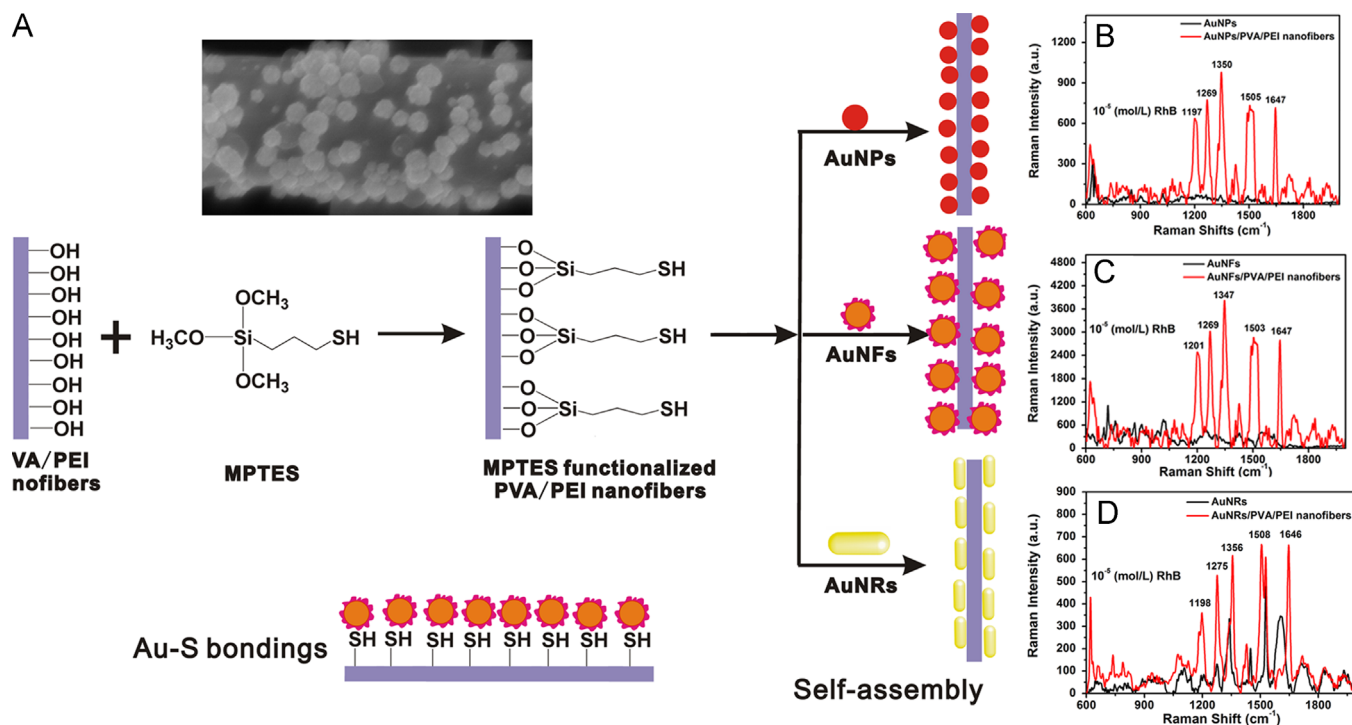


Fig. 5. (A) Schematic illustrations of the MPTES functionalization procedure of PVA/PEI nanofibers and the self-assembly process of the Au nanocrystals. SERS spectra of RhB (10^{-5} M) molecules collected on independent Au nanocrystals and the PVA/PEI nanofibers self-assembled with (B) AuNPs, (C) AuNFs, and (D) AuNRs. The inset is the FE-SEM image of AuNFs/PVA/PEI nanofiber.

effects between the AuNFs and -SH (Saha et al., 2012a; Zhu et al., 2013a). In addition, Tanaka et al. (2003) and Negishi et al. (2005) have also reported that the relatively high BEs of Au 4f was due to the binding of surface Au atoms in AuNPs with the stabilizer or passive molecules surrounding the NPs, which led to a substantial electron donation from AuNPs to the stabilizer molecules. Thus, based on the above XPS results and analysis, we can conclude that the MPTES molecules have been successfully grafted on the PVA/PEI nanofibers and a considerably larger fraction of the thiol groups coordinate to the surface of the AuNFs, indicating the formation of the strong Au-S bondings.

The schematic illustrations of the MPTES functionalization procedure of PVA/PEI nanofibers and the self-assembly process of the Au nanocrystals on MPTES functionalized PVA/PEI nanofibers are shown in Fig. 5A. In the SERS studies, a typical analyte rhodamine B (RhB) was selected as a model to demonstrate the SERS performance of these substrates. Due to the complex surface morphology of the AuNFs/(PVA/PEI) nanofibers, it is difficult to calculate an accurate enhancement factor. Fig. 5B–D shows the SERS spectra of 10^{-5} M RhB collected on different samples based on the Au nanocrystals and Au nanocrystals assembled on the PVA/PEI nanofibers, respectively. The SERS spectra of RhB based on AuNPs, AuNFs, and AuNRs all exhibit relative weaker Raman signals. After the self-assembly of the Au nanocrystals on the nanofibers, dramatic increase in Raman signals can be observed. The strong Raman signals of RhB located at 615, 1201, 1269, 1347, 1503, 1647 cm^{-1} are assigned to the C–C ring in-plane bending, C–H in-plane bending, C–O–C stretching and C–C stretching of aromatic rings (1347, 1503 and 1647 cm^{-1}), respectively, which are associated with the literatures (Zhang et al., 2005; Ahamad and Ianouli, 2011; Liu et al., 2012). Careful comparison of the SERS spectra based on different substrates, show that the Raman peaks of the RhB indicate slightly differences. It is known that there are two primary mechanisms of SERS enhancement which should be responsible for the SERS enhancements, which are electromagnetic field enhancement (EM) and chemical

enhancement (CM) (Zhang et al., 2005; Ahamad and Ianouli, 2011; Liu et al., 2012). When the RhB molecules adsorbed on the Au nanocrystals, the charge transfer between the metallic nanoparticles and adsorbed molecules can make a weak contribution to the SERS enhancements, resulting in the slight differences in Raman peaks of RhB (Gabudean et al., 2012). It should be noted that compared with the Raman intensities of the AuNPs/(PVA/PEI) and AuNRs/(PVA/PEI) nanofibers, the AuNFs/(PVA/PEI) SERS substrate demonstrates the higher Raman enhancement. According to previous studies, there are two primary mechanisms of SERS enhancement that should be responsible for the results (Qian et al., 2012; Saha et al., 2012a).

The electromagnetic effect is mostly caused on the presence of metal surfaces' roughness featured, and for a SERS substrate, the SERS-active sites ("hot" spots) are critical for the effect of SERS. It is noticeable that systems of interacting particles can produce the largest enhancements, which was recognized in early SERS research (Rycenga et al., 2011; Qian et al., 2012; Saha et al., 2012a). Compared with the single particle-based SERS substrates (AuNPs, AuNFs, and AuNRs), the Au nanocrystals assembled on nanofibers have more surface roughness than do single particles of similar size, and that means that the high densities of the assembled Au nanocrystals can create more "hot spots" at the junction positions, resulting in the intense Raman signatures of reporters. The Raman intensities of RhB based on AuNFs are higher than that on AuNPs and AuNRs, it is because compared with the AuNPs and AuNRs with smooth surfaces, the as-synthesized AuNFs possess many tips of the nanoscale bumps or the tiny cavities on the AuNFs surfaces and larger total surface area because of the roughness of the AuNFs surface, which are potential "hot" spots for the electromagnetic enhancement effects (Xie et al., 2008; Liu et al., 2012). The electromagnetic fields generated by surface plasmons depend quite intricately on the shape of the NPs, their spatial arrangement, and their environment. Combining the advantages of the AuNFs and the high densities of the "hot" spots caused by the self-assembly, it is not surprising to observe that the

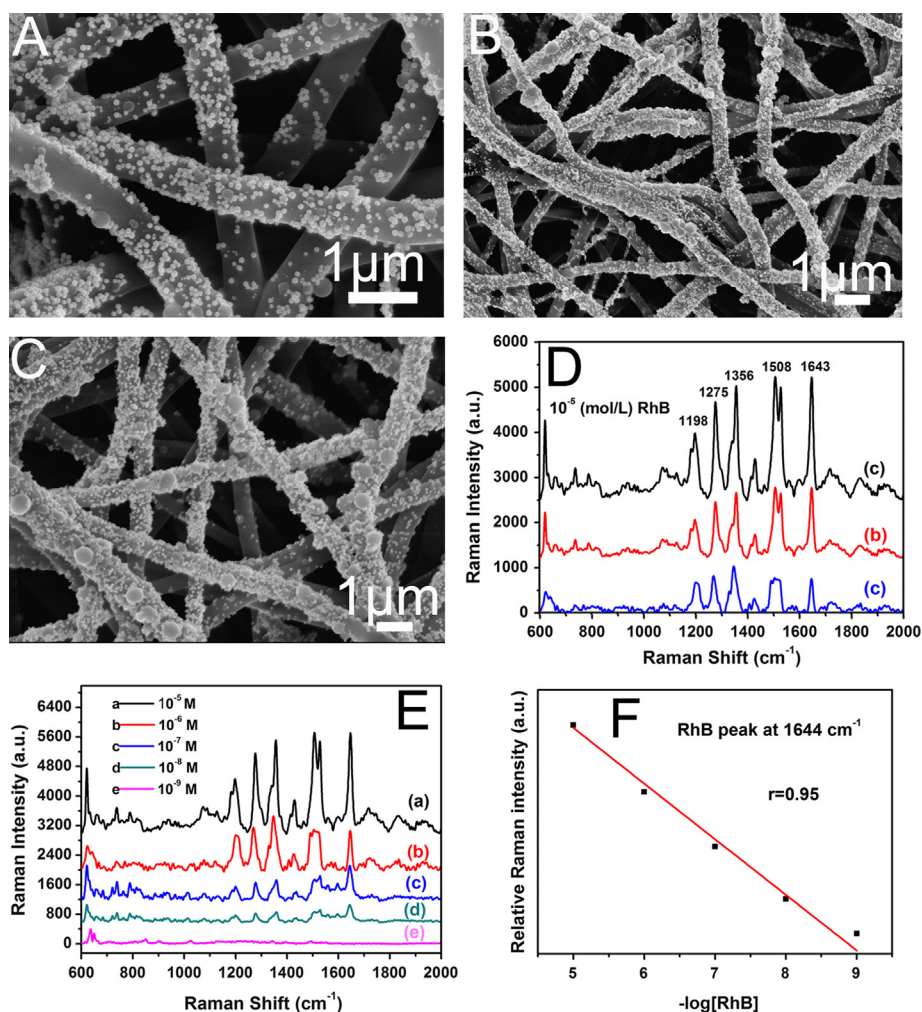


Fig. 6. FE-SEM images of the AuNFs assembled on the PVA/PEI nanofibers with increasing amounts of AuNFs solutions: (A) 5 mL (B) 10 mL and (C) 15 mL. (D) The corresponding SERS spectra of RhB (10^{-5} M) based on the AuNFs/(PVA/PEI) nanofibers with increasing amounts of AuNFs solutions: (a) 15 mL, (b) 10 mL and (c) 5 mL. (E) SERS spectra obtained from different concentrations of RhB from 10^{-5} M to 10^{-9} M using AuNFs/(PVA/PEI) nanofibers as substrates. (F) Logarithmic plot of [RhB] versus SERS intensity accompanied with linear fitting.

AuNFs/(PVA/PEI) nanofibers exhibits the highest SERS signals for RhB among the samples in our present investigations.

The above SERS results indicate that the densities of the assembled Au nanocrystals throughout the nanofibers are the key factor for the creation of “hot” spots and the SERS enhancement effects. However, [Zhang et al. \(2012b\)](#) have reported that the intensity of the Raman signal of rhodamine 6G would decreased with the increased aggregation of AgNPs on the polyacrylonitrile nanofibers, that is, with the increase of concentration of NPs, the aggregation phenomenon of NPs will increase, which would result in the decrease of SERS signal. Therefore, an optimum concentration of AuNFs assembled on the PVA/PEI nanofibers should be considered for the preparation of reliable SERS substrates.

According to the previously studies ([He et al., 2009](#); [Schlucker, 2009](#)) the AuNFs/(PVA/PEI) nanofibers with reasonable amounts of AuNFs from 5 mL to 15 mL were used as the SERS substrates for the detection of RhB. As shown in [Fig. 6A](#), at the low concentration of AuNFs solution, the AuNFs are evenly assembled throughout the PVA/PEI nanofibers, and seldom coupling AuNFs can be observed. With the increased concentration of AuNFs solution, more and more AuNFs are assembled around the nanofibers and many adjacent AuNFs start to form coupling AuNFs. When the nanofibers were nearly completely covered by the AuNFs, the AuNFs are right next to each other and create highest density “hot” spots, which are beneficial for the SERS detection efficiency. At this level of AuNFs, the nanofibers

were almost completely covered by AuNFs, and the distances between neighboring NPs are less than 10 nm, which are called “hot” spots rather than the aggregation of the AuNFs. Therefore, below 15 mL of the AuNFs, few aggregation of AuNFs can be found and the SERS intensity will not decrease.

The corresponding SERS spectra of RhB (10^{-5} M) based on the AuNFs/(PVA/PEI) substrates are shown in [Fig. 6D](#), and as expected, from curve c to curve a, the Raman signals intensities increased with the increased densities of the AuNFs and the “hot” spots. Therefore, when excited by incident light, the hot spots can contribute to larger SERS enhancement. According to the previous literatures, [Zhu et al. \(2004\)](#) have reported that the SERS intensities should depend on both size and population (i.e. interparticle distance) of NPs, and they showed that there is a threshold particle density where the interaction between the particles becomes significant ([Lee and Park, 2011](#); [Fan and Brolo, 2009](#); [Wang et al., 2006](#)). When the population is lower than this threshold, the SERS intensity increased slowly with the particle density. However, the SERS intensity will increase rapidly due to the surface plasmons coupling after the threshold value is reached ([Lee and Park, 2011](#)). The LSPR of metallic nanoparticles is the result of the collective oscillation of conduction electrons within the particles upon interaction with light ([Kundu, 2013](#)). In our present investigation, the close distance of two AuNFs leads to the interaction of their LSPR and result in the strong SERS enhancement effects.

To prove the sensitivity and reliability of AuNFs/(PVA/PEI) SERS substrates, SERS spectra of RhB were collected by varying its concentration from 10^{-5} to 10^{-9} M. As shown in Fig. 6E, from curve a to curve e, the intensities of the Raman signals of RhB decreased with the increased RhB concentrations from 10^{-5} to 10^{-9} M and 10^{-8} M RhB can still be detected with this substrate. However, the intensity of 10^{-9} M RhB is very weak, indicating the lowest detection limit of RhB. In this study, the concentration of RhB is varied and the SERS signal is decreased. It is because the decrease of RhB molecules results in the decrease of RhB molecules bound to the Au nanocrystals, and therefore, the Raman signals collected from the Au nanocrystals bonded with RhB molecules decreased. The low detection limits obtained in our SERS substrates are lower than our reported studies and the recently published literatures (Zhu et al., 2012b; Zhang et al., 2012b; Wu et al., 2010).

Fig. 6F illustrated the corresponding plot of I_{SERS} versus $-\log [R6G]$, in which I_{SERS} is the SERS intensity recorded for the band at 1644 cm^{-1} , which are the strongest bands in the R6G spectrum. The results show that the data can be fitted by a linear plot and the correlation coefficient is 0.95. The detection limit of RhB is about 10^{-9} M, which is considered as the lowest concentration leading the SERS intensity of the marker band at 1644 cm^{-1} . These SERS substrates based on PVA/PEI nanofibers with self-assembled Au nanocrystals exhibit highly efficient SERS enhancement. The Raman intensities of the detection can be easily adjusted by changing the densities of the AuNFs throughout the nanofibers. With the increased particle density of AuNFs on the nanofibers, the interparticle distances become shorter, together with the increased “hot” spots, leading to strong SERS enhancement effects. In practical applications, the water-stable SERS substrate is feasible to use as a recyclable SERS substrate.

4. Conclusions

In summary, we demonstrated a facile approach for the fabrication of flexible and reliable sulfhydryl functionalized PVA/PEI nanofibers with excellent water stability for the self-assembly of Au nanocrystals, such as AuNPs, Au nanoflowers (AuNFs), Au nanorods (AuNRs), as the highly efficient SERS substrates for the detection of RhB. Various methods were employed to cross-link the PVA nanofibers with better morphology and porous structures after immersing in water for the desired time. Various SERS-active Au nanocrystals, such as AuNPs, AuNFs, and AuNRs have been successfully synthesized. After the grafting of MPTES on the cross-linked PVA/PEI nanofibers, the Au nanocrystals can easily be self-assembled on the surfaces of the nanofibers because of the strong interactions of the Au–S chemical bondings. The amount of the AuNFs on the nanofibers can be adjusted by changing the concentration of the nanocrystals solution. Therefore, with the finely formed nanocrystals junctions, aggregates can produce intense Raman signatures of reporters with high reproducibility. The Au nanocrystals self-assembled throughout the PVA/PEI nanofibers using as SERS substrates both indicate enhanced SERS signals of RhB compared with their individual nanocrystals. It is mainly due to the close interparticle distance, mutual orientation and high density of “hot” spots, that can strongly affect the overall optical response and the SERS enhancement. By changing the amounts of the self-assembled AuNFs on the nanofibers, we can control the density of the “hot” spots and with the increased amounts of the AuNFs throughout the nanofibers, the SERS substrates show enhanced Raman signals of the RhB, indicating that the increased density of “hot” spots can directly lead to the SERS enhancement. The AuNFs/(PVA/PEI) nanofibers SERS substrates show good sensitivity, reliability and low detection limit

(10^{-9} M). The presented approach can be broadly applicable to different types of plasmonic nanostructures and these novel materials with strong SERS enhancement can be applied in bioanalysis and biosensors.

Acknowledgments

We acknowledge the support of the project of the National Natural Science Foundation of China (NSFC) (51243001 and 51373154), and the 521 Talent Project of Zhejiang Sci-Tech University.

Appendix. Supporting information

Supporting information associated with this article can be found in the online version at <http://dx.doi.org/10.1016/j.bios.2013.10.047>.

References

- Ahamad, N., Ianoul, A., 2011. *J. Phys. Chem. C* 115, 3587–3594.
- Anker, J.N., Hall, W.P., Lyandres, O., Shah, N.C., Zhao, J., Van Duyne, R.P., 2008. *Nat. Mater.* 7, 442–453.
- Aragay, G., Pino, F., Merkoci, A., 2012. *Chem. Rev.* 112, 5317–5338.
- Chen, J.J., Struk, K.N., Brennan, A.B., 2011. *Langmuir* 27, 13754–13761.
- Destaye, A.G., Lin, C.K., Lee, C.K., 2013. *ACS Appl. Mater. Interfaces* 5, 4745–4752.
- Du, X., He, J.H., 2010. *Dalton Trans.* 39, 9063–9072.
- Engel, Y., Schiffman, J.D., Goddard, J.M., Rotello, V.M., 2012. *Mater. Today* 15, 478–485.
- Fan, M.K., Brolo, A.G., 2009. *Phys. Chem. Chem. Phys.* 11, 7381–7389.
- Fan, M.K., Lai, F.J., Chou, H.L., Lu, W.T., Hwang, B.J., Brolo, A.G., 2013. *Chem. Sci.* 2013 (4), 509–515.
- Gabudean, A.M., Focsan, M., Astilean, S., 2012. *J. Phys. Chem. C* 116, 12240–12249.
- Gong, X., Bao, Y., Qiu, C., Jiang, C.Y., 2012. *Chem. Commun.* 48, 7003–7018.
- He, D., Hu, B., Yao, Q.F., Wang, K., Yu, S.H., 2009. *ACS Nano* 3, 3993–4002.
- He, F.A., Fan, J.T., Song, F., Zhang, L.M., Chan, H.L.W., 2011. *Nanoscale* 3, 1182–1188.
- He, J., Perez, M.T., Zhang, P., Liu, Y.J., Babu, T., Gong, J.H., Nie, Z.H., 2012. *J. Am. Chem. Soc.* 134, 3639–3642.
- Huang, J., Zhang, L.M., Chen, B., Ji, N., Chen, F.H., Zhang, Y., Zhang, Z.J., 2010. *Nanoscale* 2, 2733–2738.
- Jiang, G.Q., Hore, M.J.A., Gam, S., Composto, R.J., 2012. *ACS Nano* 6, 1578–1588.
- Khatri, O.P., Adachi, K., Murase, K., Okazaki, K.I., Torimoto, T., Tanaka, N., Kuwabata, S., Sugimura, H., 2008. *Langmuir* 24, 7785–7792.
- Kim, D.Y., Yu, T., Cho, E.C., Ma, Y.Y., Park, O.O., Xia, Y.N., 2011. *Angew. Chem. Int. Ed.* 50, 6328–6331.
- Kotov, N.A., 2011. *J. Mater. Chem.*, 16673–16674.
- Kundu, S., 2013. *J. Mater. Chem. C* 1, 831–842.
- Lee, C.H., Tian, L.M., Abbas, A., Kattumenu, R., Singamaneni, S., 2011. *Nanotechnology* 22, 275311–275318.
- Lee, Y.H., Park, T.G., 2011. *Langmuir* 27, 2965–2971.
- Liu, J.Y., Cai, H.B., Yu, X.X., Zhang, K., Li, X.J., Li, J.W., Pan, N., Shi, Q.W., Luo, Y., Wang, X.P., 2012. *J. Phys. Chem. C* 116, 15741–15746.
- Liu, Y.Y., Zhang, Y.X., Ding, H.L., Xu, S.C., Li, M., Kong, F.Y., Luo, Y.Y., Li, G.H., 2013. *J. Mater. Chem. A* 1, 3362–3371.
- Liu, Z., Zhou, C.S., Zheng, B.Z., Qian, L., Mo, Y., Luo, F.L., Shi, Y.L., Choi, M.M.F., Xiao, D., 2011. *Analyst* 136, 4545–4551.
- Moskovits, M., 2005. *J. Raman Spectrosc.* 36, 485–496.
- Negishi, Y., Nobusada, K., Tsukuda, T., 2005. *J. Am. Chem. Soc.* 127, 5261–5270.
- Park, K., Drummy, L.F., Wadams, R.C., Koerner, H., Nepal, D., Fabris, L., Vaia, R.A., 2013. *Chem. Mater.* 25, 555–563.
- Peng, M.F., Gao, J., Zhang, P.P., Li, Y., Sun, X.H., Lee, S.T., 2011. *Chem. Mater.* 23, 3296–3301.
- Peng, X.H., Santulli, A.C., Sutter, E., Wong, S.S., 2012. *Chem. Sci.* 3, 1262–1272.
- Perez-Juste, J., Rodriguez-Gonzalez, B., Mulvaney, P., Liz-Marzan, L.M., 2005. *Adv. Funct. Mater.* 15, 1065–1071.
- Personick, M.L., Langille, M.R., Zhang, J., Harris, N., Schatz, G.C., Mirkin, C.A., 2011. *J. Am. Chem. Soc.* 133, 6170–6173.
- Qian, K., Liu, H.L., Yang, L.B., Liu, J.H., 2012. *Nanoscale* 4, 6449–6454.
- Qiao, Y., Chen, H., Lin, Y.Y., Huang, J.B., 2011. *Langmuir* 27, 11090–11097.
- Rycenga, M., Xia, X.H., Moran, C.H., Zhou, F., Qin, D., Li, Z.Y., Xia, Y.N., 2011. *Angew. Chem. Int. Ed.* 50, 5473–5477.
- Saha, A., Palmal, S., Jana, N.R., 2012a. *Nanoscale* 4, 6649–6657.
- Saha, K., Agasti, S.S., Kim, C., Li, X.N., Rotello, V.M., 2012b. *Chem. Rev.* 112, 2739–2779.
- Sanchez-Iglesias, A., Grzelczak, M., Perez-Juste, J., Liz-Marzan, L.M., 2010. *Angew. Chem. Int. Ed.* 49, 9985–9989.
- Schlucker, S., 2009. *Chem. Phys. Chem.* 10, 1344.
- Schmit, V.L., Martoglio, R., Scott, B., Strickland, A.D., Carron, K.T., 2012. *J. Am. Chem. Soc.* 134, 59–62.

- Selegard, L., Khranovskyy, V., Soderlind, F., Vahlberg, C., Ahren, M., Kall, P.O., Yakimova, R., Uvdal, K., 2010. *ACS Appl. Mater. Interfaces* 2, 2128–2135.
- Singh, D.K., Jagannathan, R., Khandelwal, P., Abraham, P.M., Poddar, P., 2013. *Nanoscale* 5, 1882–1893.
- Song, S.P., Qin, Y., He, Y., Huang, Q., Fan, C.H., Chen, H.Y., 2010. *Chem. Soc. Rev.* 39, 4234–4243.
- Tamoto, R., Lecomte, S., Si, S., Moldovan, S., Ersen, O., Delville, M.H., Oda, R., 2012. *J. Phys. Chem. C* 116, 23143–23152.
- Tanaka, A., Takeda, Y., Imamura, M., Sato, S., 2003. *Phys. Rev. B: Condens. Matter* 68, 195415.
- Vigderman, L., Khanal, B.P., Zubarev, E.R., 2012. *Adv. Mater.* 24, 4811–4841.
- Wang, H.H., Liu, C.Y., Wu, S.B., Liu, N.W., Peng, C.Y., Chan, T.H., Hsu, C.F., Wang, J.K., Wang, Y.L., 2006. *Adv. Mater.* 18, 491–495.
- Wang, J., Yao, H.B., He, D., Zhang, C.L., Yu, S.H., 2012a. *ACS Appl. Mater. Interfaces* 4, 1963–1971.
- Wang, Y., Tang, Z.Y., Liang, X.R., Liz-Marzan, L.M., Kotov, N.A., 2004. *Nano Lett.* 4, 225–231.
- Wang, Y.Q., Yan, B., Chen, L.X., 2013. *Chem. Rev.* 113, 1391–1428.
- Wang, Z.Y., Zong, S.F., Li, W., Wang, C.L., Xu, S.H., Chen, H., Cui, Y.P., 2012b. *J. Am. Chem. Soc.* 134, 2993–3000.
- Wu, H., Lin, D.D., Pan, W., 2010. *Langmuir* 26, 6865–6868.
- Xiao, M.D., Chen, H.J., Ming, T., Shao, L., Wang, J.F., 2010. *ACS Nano* 4, 6565–6572.
- Xie, J.P., Zhang, Q.B., Lee, J.Y., Wang, D.L.C., 2008. *ACS Nano* 2, 2473–2480.
- Xie, W., Schlucker, S., 2013. *Phys. Chem. Chem. Phys.* 15, 5329–5344.
- Xie, W., Herrmann, C., Kompe, K., Haase, M., Schlucker, S., 2011. *J. Am. Chem. Soc.* 133, 19302–19305.
- Ye, X.C., Jin, L.H., Caglayan, H., Chen, J., Xing, G.Z., Zheng, C., Doan-Nguyen, V., Kang, Y.J., Engheta, N., Kagan, C.R., Murray, C.B., 2012. *ACS Nano* 6, 2804–2817.
- Yoon, I., Kang, T., Choi, W., Kim, J., Yoo, Y., Joo, S.W., Park, Q.H., Ihee, H., Kim, B., 2009. *J. Am. Chem. Soc.* 131, 758–762.
- Yuan, J.Y., Gao, H.T., Schacher, F., Xu, Y.Y., Richter, R., Tremel, W., Muller, A.H.E., 2009. *ACS Nano* 3, 1441–1450.
- Zhang, C.L., Lv, K.P., Cong, H.P., Yu, S.H., 2012a. *Small* 8, 648–653.
- Zhang, F.Z., Zhao, X.F., Feng, C.H., Li, B., Chen, T., Lu, W., Lei, X.D., Xu, S.L., 2011. *ACS Catal.* 1, 232–237.
- Zhang, J.T., Li, X.L., Sun, X.M., Li, Y.D., 2005. *J. Phys. Chem. B* 109, 12544–12548.
- Zhang, L.F., Gong, X., Bao, Y., Zhao, Y., Xi, M., Jiang, C.Y., Fong, H., 2012b. *Langmuir* 28, 14433–14440.
- Zhang, T.J., Wang, W., Zhang, D.Y., Zhang, X.X., Ma, Y.R., Zhou, Y.L., Qi, L.M., 2010. *Adv. Funct. Mater.* 20, 1152–1160.
- Zhu, H., Du, M.L., Yu, D.L., Wang, Y., Zou, M.L., Xu, C.S., Fu, Y.Q., 2012a. *Dalton Trans.* 41, 13795–13799.
- Zhu, H., Du, M.L., Zou, M.L., Xu, C.S., Fu, Y.Q., 2012b. *Dalton Trans.* 41, 10465–10471.
- Zhu, H., Du, M.L., Zou, M.L., Xu, C.S., Li, N., Fu, Y.Q., 2012c. *J. Mater. Chem.* 22, 9301–9307.
- Zhu, H., Du, M.L., Yu, D.L., Wang, Y., Wang, L.N., Zou, M.L., Zhang, M., Fu, Y.Q., 2013a. *J. Mater. Chem. A* 1, 919–929.
- Zhu, H., Du, M.L., Zhang, M., Wang, P., Bao, S.Y., Wang, L.N., Fu, Y.Q., Yao, J.M., 2013b. *Biosens. Bioelectron.* 43, 210–215.
- Zhu, H., Du, M.L., Zhang, M., Wang, P., Bao, S.Y., Fu, Y.Q., Yao, J.M., 2013c. *Sensor. Actuat. B – Chem.* 185, 608–619.
- Zhu, Z.H., Zhu, T., Liu, Z.F., 2004. *Nanotechnology* 15, 357–364.
- Zou, M.L., Du, M.L., Zhu, H., Xu, C.X., Fu, Y.Q., 2012. *J. Phys. D: Appl. Phys.* 45, 325302–325308.
- Zou, M.L., Du, M.L., Zhu, H., Xu, C.S., Li, N., Fu, Y.Q., 2013. *Polym. Eng. Sci.* 53, 1099–1108.